Journal of Metals, Materials and Minerals, 36(1), e2488, 2026

Dual-functional activated carbon from coffee grounds for crystal violet dye removal and subsequent application as an electrode material in energy storage devices

Sirikorn KHAOPHONG[1], Tawatchai KANGKAMANO[1], Sonchai INTACHAI[1,2], and Panita KONGSUNE[1,2,*]

[1] *Department of Chemistry, Faculty of Science and Digital Innovation, Thaksin University, Phattalung, 93210, Thailand*
[2] *Innovative Material Chemistry for Environment Center, Thaksin University, Phattalung, 93210, Thailand*

***Corresponding author e-mail**: dpanita@tsu.ac.th

Received date:
7 August 2025
Revised date:
9 September 2025
Accepted date:
6 October 2025

Keywords:
Spent coffee grounds;
Activated carbon;
Crystal violet;
Supercapacitor electrode;
Biomass valorization

Abstract

The conversion of agricultural waste into high-value functional materials offers a sustainable strategy to address environmental concerns. In this study, activated carbon was synthesized from spent coffee grounds (CGAC) via KOH activation and used for crystal violet (CV) dye adsorption. Under optimal conditions (0.5 g dosage, 300 mg·L^{-1} CV, 30°C, 120 min), CGAC achieved 91.41% removal efficiency, with adsorption behavior fitting pseudo-second-order kinetics and the Freundlich isotherm. Thermo-dynamic parameters confirmed a spontaneous and endothermic process. Moreover, the reusability study revealed that CGAC maintained a high removal efficiency above 88% after seven adsorption–desorption cycles, demonstrating its structural stability and potential for practical wastewater treatment. Notably, the dye-saturated carbon was further processed into electrode materials through five different preparation routes: unmodified CGAC, dye-loaded CGAC (CGAC_CV), hydro-thermally treated (CGAC_CV_H), thermally treated (CGAC_CV_600), and combined hydrothermal-thermal treated (CGAC_CV_H600). Among them, CGAC_CV_H600 exhibited the best electrochemical performance with a specific capacitance of 326.4 F·g^{-1} at 0.25 A·g^{-1} in 6 M KOH due to its optimized porosity and nitrogen/oxygen doping. This study is among the few that explore the reuse of dye-laden adsorbents through systematic post-treatment strategies, offering a circular and sustainable pathway for biomass-derived carbon in both environmental remediation and energy storage.

1. Introduction

In the pursuit of sustainable and eco-friendly energy storage solutions, the development of advanced electrode materials plays a pivotal role. Electrochemical capacitors, or supercapacitors, have garnered significant attention due to their high-power density, rapid charge-discharge capabilities, and long cycle life [1-4]. Generally, supercapacitors are classified into electrical double layer capacitors (EDLCs) and pseudocapacitors (PCs) [5,6]. PCs store energy via reversible faradaic reactions at the surface of active materials, whereas EDLCs rely on the electrostatic separation of charges at the electrode-electrolyte interface, a mechanism largely governed by the surface area and porosity of the electrode materials [7,8]. Hence, optimizing the physicochemical structure of carbon-based electrodes is vital for improving the capacitance and energy storage performance of EDLCs [7-9].

Activated carbon (AC) is one of the most widely used electrode materials in commercial supercapacitors, primarily due to its high specific surface area, well-developed porous structure, electrical conductivity, and low production cost [10-12]. Biomass-derived AC has gained attention as a sustainable and low-cost alternative to conventional carbon materials [9,13]. Agricultural waste, such as coconut shells [14], loofah sponge [15], and eucalyptus bark [16], has been successfully converted into high-performance ACs with specific capacitance values exceeding 250 F·g^{-1} under alkaline conditions [10,17,18]. However, the energy storage performance of biomass-derived AC is often limited by the inherent electrostatic nature of EDLC mechanisms.

To overcome this limitation, surface modification through heteroatom doping-such as nitrogen, sulfur, and phosphorus-has been employed to introduce pseudocapacitive behavior into AC materials [19-22]. Co-doping strategies have demonstrated significant improvements in specific capacitance by enhancing redox activity and charge transfer at the electrode-electrolyte interface [19-22]. In addition to chemical doping, physical adsorption of functional molecules-such as organic dyes-can also introduce heteroatoms and alter the surface chemistry of AC.

Among various applications, AC is extensively used as an adsorbent for water treatment due to its exceptional adsorption capabilities toward organic dyes, heavy metals, and other pollutants [23-25]. Crystal violet (CV), a common cationic dye, is effectively removed from aqueous solutions by AC via electrostatic interactions and π–π stacking mechanisms [26-30]. Interestingly, during the adsorption process, dye molecules such as CV can introduce nitrogen and oxygen-containing groups onto the AC surface, thereby potentially modifying its surface functionality and enhancing its electrochemical performance [26,31,32]. Despite the widespread use of AC in dye adsorption, few studies have explored the reutilization of spent dye-loaded AC as

electrode materials in supercapacitors. The integration of dye adsorption and energy storage applications offers a dual-functional and zero-waste approach: not only treating dye-contaminated wastewater but also valorizing the spent adsorbent into high-performance energy storage materials. This strategy aligns with the principles of circular economy and sustainable materials engineering.

In this study, activated carbon was synthesized from coffee ground biomass waste (CGAC), and subsequently utilized for crystal violet (CV) adsorption. The adsorbed CV introduced nitrogen hetero-atoms onto the CGAC surface, potentially enhancing its electro-chemical performance. To systematically investigate the effect of dye adsorption and post-treatment conditions on electrode properties, five different electrode materials were prepared as (1) untreated coffee-ground activated carbon (CGAC), (2) CGAC after CV adsorption (CGAC_CV), (3) CV-adsorbed CGAC further thermally treated at 600℃ (CGAC_ CV_600), (4) CV-adsorbed CGAC subjected to hydrothermal treatment at 140°C for 24 h (CGAC_CV_H), and (5) CV-adsorbed CGAC treated hydrothermally at 140℃ for 24 h followed by thermal treatment at 600℃ (CGAC_CV_H600). The structural, compositional, and electrochemical properties of these samples were characterized and evaluated to determine the optimal strategy for enhancing electrode performance. This dual-functional approach demonstrates a sustainable pathway to upcycle biomass-derived AC for both environmental remediation and electrochemical energy storage applications.

2. Experimental details

2.1 Chemicals and reagents

Coffee grounds were collected from Thaksina Café, Thaksin University, Phatthalung Province, Thailand. Potassium hydroxide (KOH, 85%), nitric acid (HNO_3, 94%), and hydrochloric acid (HCl, 36%) were purchased from Elago Enterprises Pty Ltd., Victoria, Australia. Crystal violet dye ($C_{25}N_3H_{30}Cl$, 88%) was obtained from Loba Chemie Pvt. Ltd., Mumbai, India. NafionTM 117 solution (5 wt%) was acquired from Sigma-Aldrich Pty Ltd., St. Louis, MO, USA. Ethanol (C_2H_6O, 99.8%) was purchased from E. Merck, Darmstadt, Germany. All reagents were used without further purification.

2.2 Preparation of coffee ground activated carbon (CGAC)

The collected coffee grounds were oven-dried at 105°C for 24 h to remove moisture. The dried material was then mixed with 85% KOH and deionized water in a 1:1 weight ratio. After thorough mixing, the sample was left to soak at room temperature for 24 h. The impregnated biomass was transferred into a crucible and carbonized at 600°C for 4 h. The resulting material was washed with deionized water until a neutral pH was achieved (pH ~7), aided by mild nitric acid washing. The washed sample was dried again at 105°C for 24 h to obtain the coffee ground activated carbon (CGAC).

2.3 Characterization of CGAC

The surface morphology of the activated carbon samples was analyzed using a field emission environmental scanning electron microscope (FESEM, Quanta 450 FEG, Switzerland). Elemental composition and distribution were determined by Energy dispersive X-ray spectroscopy (EDS). Surface functional groups were characterized using Fourier transform infrared spectroscopy (FTIR, ATR-FTIR G8044AA, Agilent Technologies) in the range of 650 cm^{-1} to 4000 cm^{-1}. The Brunauer-Emmett-Teller (BET) method was employed to determine the specific surface area, while pore size distribution was analyzed using the Barrett-Joyner-Halenda (BJH) model.

2.4 Batch adsorption experiment

The effects of absorbent dose, initial concentration of crystal violet solution, pH of Crystal violet solution, temperature, and absorption equilibrium time were studied and optimized. The effects of parameters on the kinetics, isotherms, and thermodynamic parameters of the crystal violet solution on absorption were studied. The CGAC of 0.1 g to 0.8 g was soaked in 150 mL of 100 $mg{\cdot}L^{-1}$ to 400 $mg{\cdot}L^{-1}$ of crystal violet solution for a duration of 15 min to 180 min at 30°C to 50°C, set at 240 rpm. The initial and final concentrations of crystal violet were analyzed by a UV-Visible spectrophotometer at 590 nm.

The removal percentages (% removal) and equilibrium adsorption capacity (q_e) of crystal violet were calculated using the following Equation (1) and Equation (2), respectively.

$$q_e = \left(\frac{C_0 - C_e}{m}\right) \times V \quad (1)$$

$$\%\ \text{Removal} = \left(\frac{C_0 - C_e}{C_0}\right) \times 100 \quad (2)$$

where C_0 ($mg{\cdot}L^{-1}$) and C_e ($mg{\cdot}L^{-1}$) are the initial and final concentration of crystal violet in the solution before and after adsorption, respectively. V (L) is the solution volume and m (g) is the mass of adsorbent.

2.5 Electrode preparation and electrochemical measurements

To evaluate the effects of dye adsorption and post-treatment processes on electrochemical performance, five types of electrode materials were prepared as (i) CGAC (coffee ground activated carbon), (ii) CGAC_CV (CGAC after CV adsorption), (iii) CGAC_CV_600 (CGAC_CV thermally treated at 600°C), (iv) CGAC_CV_H (CGAC_ CV subjected to hydrothermal treatment at 140°C for 24 h), and (v) CGAC_CV_H600 (CGAC_CV treated hydrothermally at 140°C for 24 h and subsequently calcined at 600°C). Electrodes were fabricated by preparing a suspension composed of 0.005 g of active material, 0.05 mL of 5 wt% Nafion solution, 0.66 mL of isopropanol, and 0.29 mL of deionized water. The suspension was drop-cast onto a glassy carbon electrode (GCE) with a geometric surface area of 0.0707 cm^2 and dried at 30°C for 12 h. Electrochemical measurements were carried out using a three-electrode system connected to an Autolab PGSTAT101 electrochemical workstation (Metrohm, Switzerland), with an Ag/AgCl electrode as the reference and a platinum wire as the counter electrode. A 6 M KOH solution was used as an electrolyte. Cyclic voltammetry (CV) was performed at scan rates ranging from 0.1 $V{\cdot}s^{-1}$ to 1.0 $V{\cdot}s^{-1}$, and galvanostatic charge-discharge (GCD) testing was conducted at current densities ranging from 0.25 $A{\cdot}g^{-1}$ to 1.0 $A{\cdot}g^{-1}$ within a voltage window of –0.2 V to 0.1 V [33].

3. Results and discussion

3.1 Surface properties and elemental composition of AC samples

The physicochemical properties of the five activated carbon (AC) samples, including surface area, pore volume, pore diameter, and elemental composition (% atomic) are summarized in Table 1. These properties are crucial in determining the electrochemical performance of the materials, particularly for their application in electric double-layer capacitors (EDLCs). The CGAC exhibited a surface area of 396.84 $m^2 \cdot g^{-1}$, a pore volume of 0.20 $cm^3 \cdot g^{-1}$, and an average pore diameter of 1.61 nm, indicating its suitability as a mesoporous material for ion transport. Upon adsorption of crystal violet (CGAC_CV), the surface area and pore volume decreased to 296.58 $m^2 \cdot g^{-1}$ and 0.14 $cm^3 \cdot g^{-1}$, respectively. This reduction suggests partial pore blockage by the dye molecules and surface modification, which also reflects in the increase of nitrogen (N) content to 7.63 at% originating from the amine groups of crystal violet. Interestingly, the hydrothermal treatment of the dye-loaded sample (CGAC_CV_H) further reduced the surface area and pore volume to 248.70 $m^2 \cdot g^{-1}$ and 0.11 $cm^3 \cdot g^{-1}$, respectively, while maintaining a comparable pore diameter (1.69 nm). The nitrogen content decreased to 4.00%, likely due to the partial decomposition of CV under hydrothermal conditions. This mild treatment did not significantly alter the pore structure but affected the surface chemistry. In contrast, thermal treatment at 600°C (CGAC_CV_600) resulted in a remarkable increase in surface area to 436.90 $m^2 \cdot g^{-1}$ and pore volume to 0.22 $cm^3 \cdot g^{-1}$, similar to that of pristine CGAC. This increase suggests that heat treatment effectively removed loosely bound dye molecules and regenerated the porosity. However, the nitrogen content dropped to 3.16%, indicating the degradation of organic dye structures under high temperature.

The combination of hydrothermal and thermal treatment (CGAC_CV_H600) yielded the highest surface area of 471.32 $m^2 \cdot g^{-1}$ and a pore volume of 0.24 $cm^3 \cdot g^{-1}$, with a consistent pore diameter of 1.61 nm. The nitrogen content further decreased to 2.98 at%, yet the material retained considerable heteroatom doping and the highest surface area among all samples. This suggests a synergistic effect between the two treatments, enhancing porosity while partially preserving surface functionalities introduced by CV [34].

Elemental analysis via EDS revealed that all samples consisted primarily of carbon (C) and oxygen (O), with trace amounts of nitrogen and other elements. The presence of nitrogen, which was absent in the original CGAC, confirmed the successful doping of heteroatoms through dye adsorption and subsequent treatments. Such doping is known to introduce capacitive behavior, potentially improving electrochemical performance by providing additional active sites for charge storage.

These results demonstrate that post-treatment strategies significantly influence the surface area, pore characteristics, and elemental composition of dye-loaded AC, thereby affecting their potential as high-performance electrode materials for energy storage applications.

3.2 Morphological, chemical, and surface charge characteristics of adsorbents

The SEM image of CGAC (Figure 1(a)) displays an irregular and highly porous surface structure, which is typical of activated carbon and favorable for adsorption due to the high surface area and pore accessibility. After CV dye adsorption (Figure 1(b)), the surface of CGAC_CV becomes more compact with partially filled or blocked pores, suggesting physical occupation of the pores by dye molecules and possible surface interactions. This indicates successful dye immobilization onto the carbon matrix. Upon further hydrothermal treatment and carbonization at 600°C (CGAC_CV_H600; Figure 1(c)), the structure appears more interconnected and organized, with reopened pores and smoother pore walls, which may improve diffusion paths and structural stability for subsequent applications. The elemental mapping of CGAC_CV (Figure 1(d)) confirms the homogeneous distribution of carbon (C), oxygen (O), and nitrogen (N) throughout the material. The presence of nitrogen, which is absent in the pristine CGAC, indicates the successful incorporation of nitrogen-containing groups, likely originating from the CV dye. These nitrogen functionalities are known to enhance adsorption affinity and potentially improve electrochemical performance by increasing surface polarity and redox-active sites.

FTIR spectra of CG, CGAC, and CGAC_CV are shown in Figure 1(e). Raw coffee grounds (CG) exhibit prominent peaks around 2850 cm^{-1} to 2950 cm^{-1} (C–H stretching), ~1700 cm^{-1} (C=O stretching in esters), and ~1030 cm^{-1} (C–OH stretching), indicating lignocellulosic content. Upon activation (CGAC), these peaks shift or diminish, and new bands appear at 1620 cm^{-1} (C=C), 1250 cm^{-1} (asymmetric C–O–C), 1030 cm^{-1} (C–OH), and 600 cm^{-1} to 700 cm^{-1} (C–H bending), confirming structural decomposition and formation of new oxygenated functionalities. After CV adsorption (CGAC_CV), the spectra remain generally similar, but a weak band near 1700 cm^{-1} reappears, suggesting the presence of dye molecules, particularly C=O groups from CV, confirming successful surface interaction without substantial alteration of the carbon backbone.

Table 1. Surface area, pore volume, average pore diameter, and elemental composition (% atomic by EDS) of activated carbon samples before and after dye adsorption and thermal treatment.

Adsorbents	Surface arears	Pore volume	DFT pore diameter	% Atomic			
	[$m^2 \cdot g^{-1}$]	[$cm^2 \cdot g^{-1}$]	[nm]	C	O	N	others
CGAC	396.84	0.20	1.61	86.68	12.83	-	0.49
CGAC_CV	296.58	0.14	1.69	83.27	8.35	7.63	0.75
CGAC_CV_H	248.702	0.11	1.69	87.42	8.31	4.00	0.26
CGAC_CV_600	436.90	0.22	1.61	87.92	6.85	3.16	2.08
CGAC_CV_H600	471.32	0.24	1.61	87.67	8.30	2.98	1.05

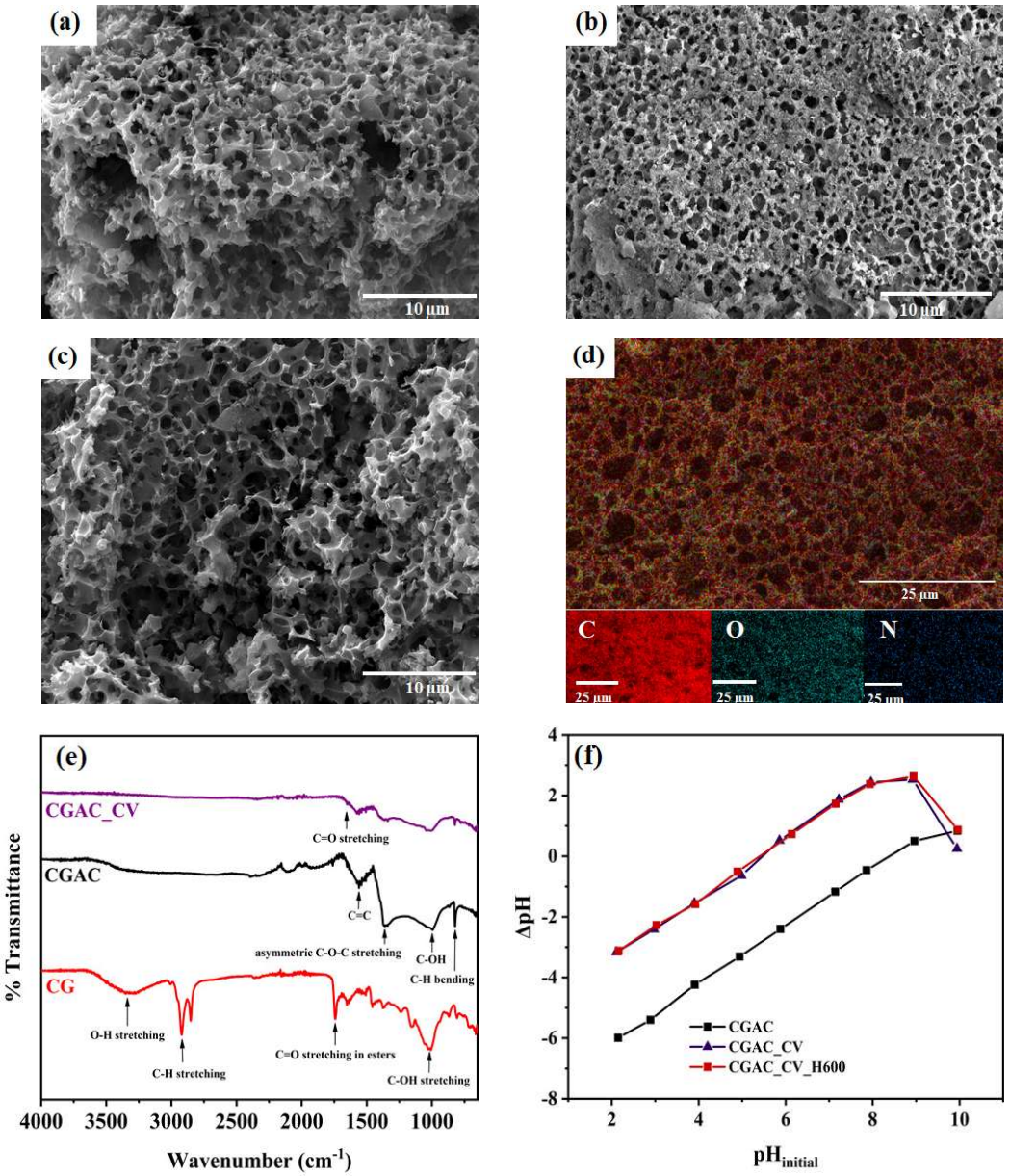

Figure 1. Structural and physicochemical characterization of CG-based adsorbents, including (a-c) surface morphology (SEM), (d) elemental mapping (EDS), (e) functional group identification (FTIR), and (f) point of zero charge (pH_{pzc}) analysis.

The point of zero charge (pH_{pzc}) results (Figure 1(f)) illustrates the impact of surface modification on surface acidity. The CGAC sample shows a pH_{pzc} of 8.58, indicating a basic surface, favorable for adsorbing acidic or anionic species at lower pH. After dye adsorption, the pH_{pzc} of CGAC_CV decreases to 5.88, suggesting the introduction of acidic or negatively charged groups such as sulfonates or nitrogen-containing moieties from CV. Upon hydrothermal carbonization treatment, CGAC_CV_H600 exhibits a further reduction in pH_{pzc} to 4.97, indicating a more acidic surface that is likely enriched in oxygen and nitrogen functionalities. A lower pH_{pzc} implies a predominantly negative surface charge at neutral pH, enhancing the material's potential in electrochemical and dye adsorption applications.

The transformation of CG-based adsorbents involves a sequence of modifications that enhance both adsorption and electrochemical performance. During CV adsorption, electrostatic attraction, hydrogen bonding, and π–π interactions occur between the dye and polar functional groups (–COOH, –OH) on CGAC, leading to surface compaction via pore blockage. Subsequent hydrothermal treatment and carbonization at 600°C (CGAC_CV_H600) promote pore reopening, matrix rearrangement, and the stabilization of nitrogen- and oxygen-containing groups. These functionalities enhance surface polarity and redox activity, which are crucial for adsorption and energy storage.

3.3 Influence of adsorbent dose, initial concentration, contact time, temperature, and reusability of CGAC on CV adsorption

Results from the study of the effects of adsorbent dosage, CV initial concentration, adsorption temperature, and contact time on CV adsorption are displayed in Figure 2, respectively. Figure 2(a) presents the effect of adsorbent dose on CV adsorption, with varying adsorbent amounts from 0.1 g to 0.8 g for CGAC, at fixed times of 60 min, room temperature, and initial concentrations of 300 $mg \cdot g^{-1}$. It was

observed that the amount of CV adsorbed per unit weight of adsorbent (q) decreased with an increase in adsorbent dose, while the removal percentage of CV by CGAC slightly increased with an increase in adsorbent dose. This suggests that using 0.5 g of CGAC can yield a high value of q and CV removal.

The effects of initial CV concentration on the adsorption capabilities of the CGAC to CV dye were systematically studied using a specific amount of CGAC (0.5 g/150 mL) and varying concentration levels (100 $mg \cdot L^{-1}$ to 400 $mg \cdot L^{-1}$). Figure 2(b) contains the trends of the CGAC adsorption capacities (q, $mg \cdot g^{-1}$) for the adsorption of the CV dye at various CV concentrations. Figure 2(b) shows that by changing CV dye concentrations from 100 $mg \cdot L^{-1}$ to 400 $mg \cdot L^{-1}$, the amount of CV dye molecules absorbed on the surface of CGAC expanded from 28.19 $mg \cdot g^{-1}$ to 111.52 $mg \cdot g^{-1}$. This is explained by the greater concentration gradient, which acts as a motivator to drive adsorption of the CV dyes onto the CGAC active sites [35].

The effect of pH on the adsorption of CV on CGAC is shown in Figure 2(c), it can be explained based on pH_{pzc} (Figure 1(f)), the pH_{pzc} of CGAC is 8.6, at pH < pH_{pzc} the adsorbent surface is positively charged due to the high concentration of H_3O protons in solution, which induces their competition with the cationic dye and causes a repulsive force between the dye ions and sites on the adsorbent surface. However, at pH > pH_{pzc}, the number of negative charges of OH– increases and favors cation binding (CV) due to electrostatic attraction forces [36]. Figure 2(c) shows that at pH 4, the maximum quantity adsorbed is obtained, allowing us to identify it as the optimal pH for the rest of the parametric study.

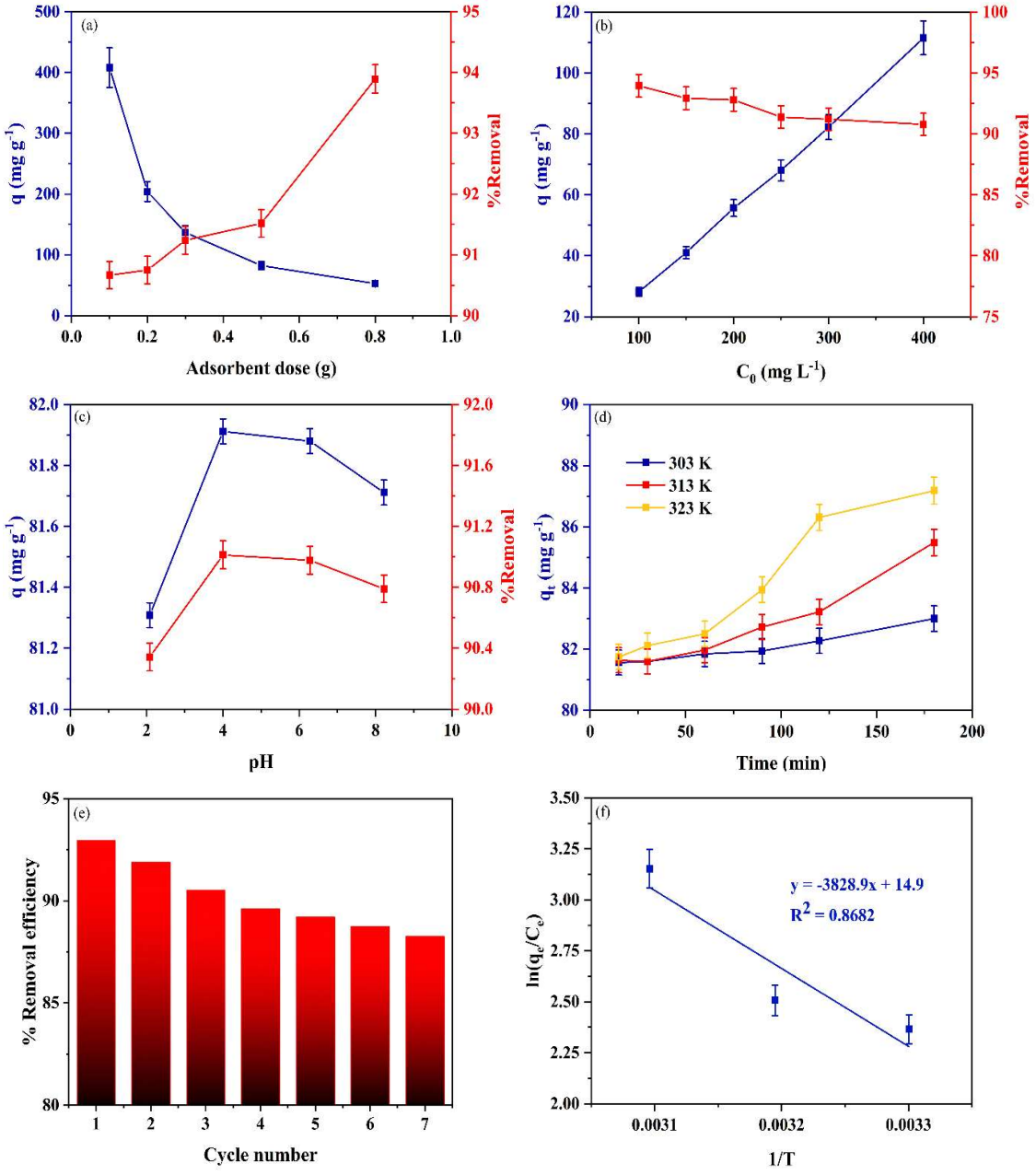

Figure 2. The effects of (a) adsorbent dosage, (b) initial CV concentration, (c) pH, (d) time, (e) reusability, and (f) temperature on the adsorption capacity of CV onto the CGAC adsorbent.

The study on the adsorption equilibrium time and temperature was conducted using an adsorbent dosage of 0.5 g, a CV concentration of 300 mg·L^{-1}, and the initial pH of the dye solution. It was found that the adsorption equilibrium was reached at 120 min, as shown in Figure 2(d). The adsorption capacities at temperatures of 303 K, 313 K, and 323 K were 82.27 mg·g^{-1}, 83.22 mg·g^{-1}, and 86.31 mg·g^{-1}, respectively. The equilibrium was reached more quickly as the temperature increased. The study on the effect of temperature on adsorption capacity revealed that increasing the temperature enhanced the adsorption process, indicating that the adsorption is an endothermic process.

3.4 Reusability of CGAC on CV adsorption

The reusability of an adsorbent is a critical factor for its practical application in wastewater treatment. To evaluate this property, regeneration and reusability studies of CGAC for crystal violet (CV) adsorption were carried out over seven consecutive adsorption–desorption cycles (Figure 2(e)). The initial removal efficiency of CGAC was approximately 93% in the first cycle. A gradual decrease in performance was observed with repeated use, which can be attributed to the incomplete desorption of dye molecules and partial blocking of active sites after each regeneration step. After the seventh cycle, the removal efficiency remained as high as ~88%, indicating that CGAC retained most of its adsorption capacity despite repeated operation.

The relatively small reduction in efficiency over multiple cycles highlights the structural stability and robustness of CGAC. The gradual decline can be ascribed to irreversible adsorption of CV molecules within micropores or strong interactions with surface functional groups, which reduce the availability of active sites during subsequent cycles. Similar reusability behavior has been reported in other bio-based activated carbons, where a slight decrease in adsorption efficiency is generally unavoidable due to pore blockage and fouling effects.

3.5 Adsorption thermodynamics

The estimation of the standard change in thermodynamic properties such as enthalpy (ΔH°), Gibbs free energy (ΔG°), and entropy (ΔS°) highlights the driving forces for the CV adsorption pathway with CGAC, whether it is enthalpic or entropic in origin. Then, the thermodynamic characteristics ΔG°, ΔH°, and ΔS°, and the thermodynamic equilibrium factor (K_L; the unit of K_L must be dimensionless; therefore, the relation was multiplied by the density of the liquid (1 g·L^{-1})), were derived using Equation (3-5) [37].

Based on the regression parameters of the linear van't Hoff plot, ΔS° and ΔH° were estimated from the intercept and slope terms and ΔG° was estimated by Equation (3), as listed in Table 2. The results obtained (Table 2) for the ΔG° at 303 K, 313 K, and 323 K are –37.50 kJ·mol^{-1}, –38.74 kJ·mol^{-1}, and –39.98 kJ·mol^{-1} respectively, which highlights the spontaneous adsorption route of CV [38]. The positive value of ΔH° (31.79 kJ·mol^{-1}) states that the CGAC uptake of CV dye species is endothermic [38]. Additionally, when the CV adsorption process is underway, a positive value (123.88 J·mol^{-1} K^{-1}) for ΔS° implies that the process is entropy driven, according to greater randomness at the CGAC-liquid interface.

Table 2. Parameters of the kinetic pseudo-first-order, pseudo-second order, Langmiur, Freundlich, Temkin, Dubinin-Radushkevich (D-R) isotherms and Thermodynamic of CGAC adsorbents on crystal violet adsorption.

Model/Equation		**Parameters**		
Adsorption		q_{exp} [mg·g^{-1}]		82.27
Thermodynamic				
$\Delta G° = -RTlnK_L$	….. (3)	ΔH° [kJ·mol^{-1}]		31.79
$K_L = \frac{q_e}{c_e}$	….. (4)	ΔS° [J·mol^{-1}·K]		123.88
			303 K	–37.50
$lnK_L = \frac{\Delta H°}{RT} - \frac{\Delta S°}{R}$	….. (5)	ΔG° [kJ·mol^{-1}]	313 K	–38.74
			323 K	–39.98
Kinetic models				
Pseudo-first order		q_{cal} [mg·g^{-1}]		0.7226
$\ln(q_e - q_t) = \ln q_e - k_1 t$	….. (6)	K [min^{-1}]		0.0253
		R^2		0.9628
Pseudo-second order		q_{cal} [mg·g^{-1}]		83.33
$\frac{1}{q_t} = \frac{1}{k_2 q_e^2} + \frac{t}{q_e}$	….. (7)	K [min^{-1}]		0.0169
		R^2		0.9999
Isotherm models				
Langmuir		K_L [L·mg^{-1}]		0.0863
$\frac{C_e}{q_e} = \frac{1}{q_m K_L} + \frac{C_e}{q_m}$	….. (8)	q_m [mg·g^{-1}]		151.52
		R^2		0.8917
Freundlich		K_F [L·mg^{-1}]		0.2560
$\ln q_e = \ln K_F + \frac{1}{n}\ln C_e$	….. (9)	n		1.9186
		R^2		0.9712
Temkin		K_T [L·mg^{-1}]		1.0023
$q_e = B_1 \ln k_T + B_1 \ln C_e$	….. (10)	B_1		32.7584
		R^2		0.8984
D-R		K_D [L·mg^{-1}]		1.5397
$E = \frac{1}{\sqrt{2K_D}}$	….. (11)	E		0.5699
		R^2		0.7516
When ***$\ln q_e = \ln q_m - K_D\varepsilon^2$ ….. (12), $\varepsilon = RT\ln\left(1 + \frac{1}{C_e}\right)$ ….. (13)				

3.6 Adsorption kinetics

The dynamics of the adsorption process provide insight into the variables that influence the rate of adsorption and the interactions between the CGAC and the CV. Two kinetic models, including the pseudo-first order and pseudo-second order models were investigated to assess the mechanism of the CV adsorption process by the CGAC (Figure 3(a-b)). Table 2 displays the mathematical formulae for each of these models, whilst the findings of kinetic parameters are listed in Table 2. The large R^2 values of pseudo-second order in comparison to pseudo-first order depict that the pseudo-second order model is well suited to describe CV adsorption performance onto CGAC. Furthermore, the great match of $q_{e(cal)}$ generated from the pseudo-second order model with the $q_{e(exp)}$ shows that the pseudo-second order model accounts for the adsorption rate of CV uptake by the adsorbent. This assumes that chemisorption is the rate-limiting step in the adsorption of CV onto CGAC, which comprises the electron sharing between the CV molecules and the CGAC active sites [39].

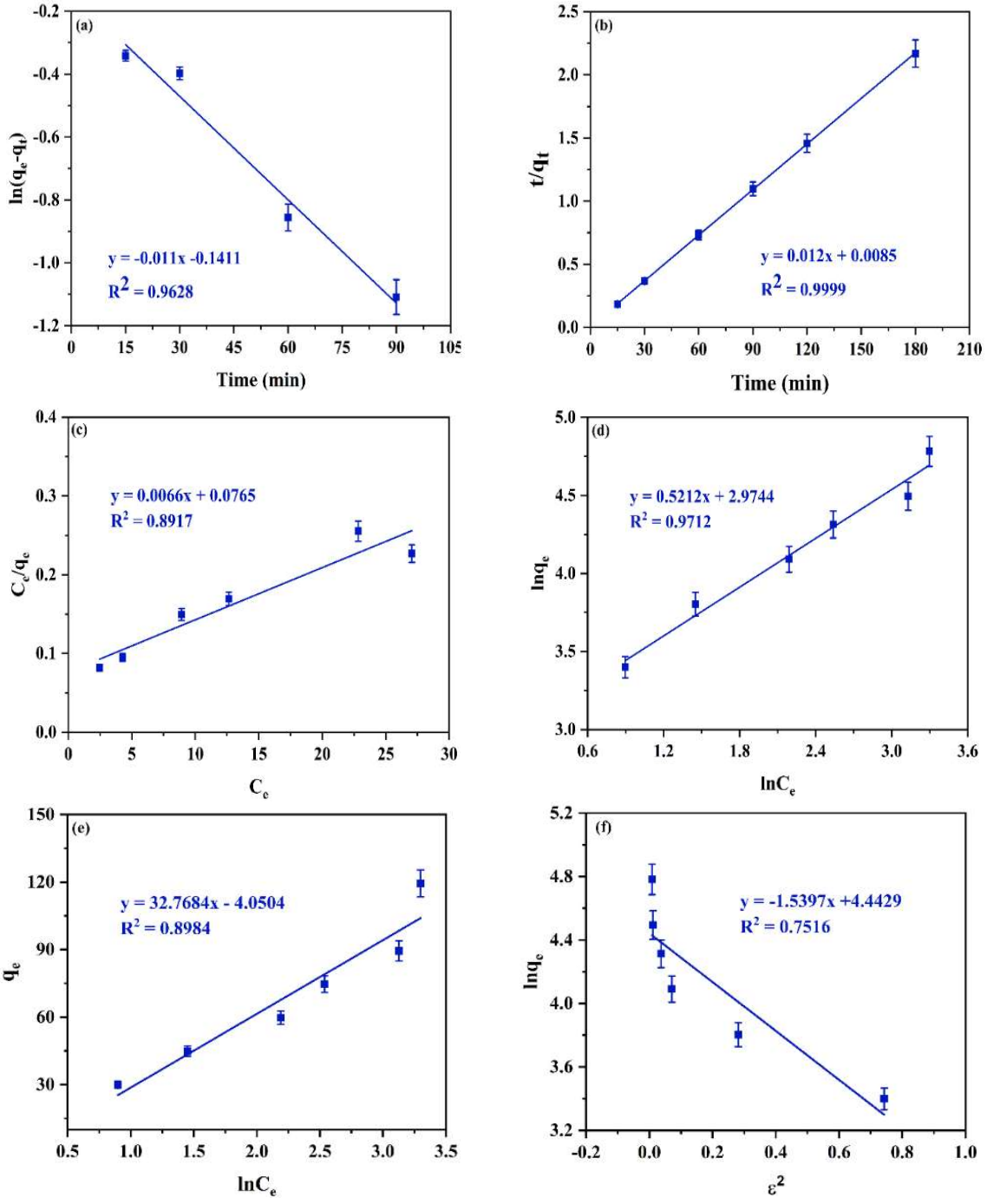

Figure 3. Kinetics and Isotherm plots of (a) pseudo-first order, (b) pseudo-second order, (c) Langmuir, (d) Freundlich, (e) Temkin, and (f) Dubinin-Radushkevich (D-R) models on crystal violet adsorption capacity by CGAC adsorbents.

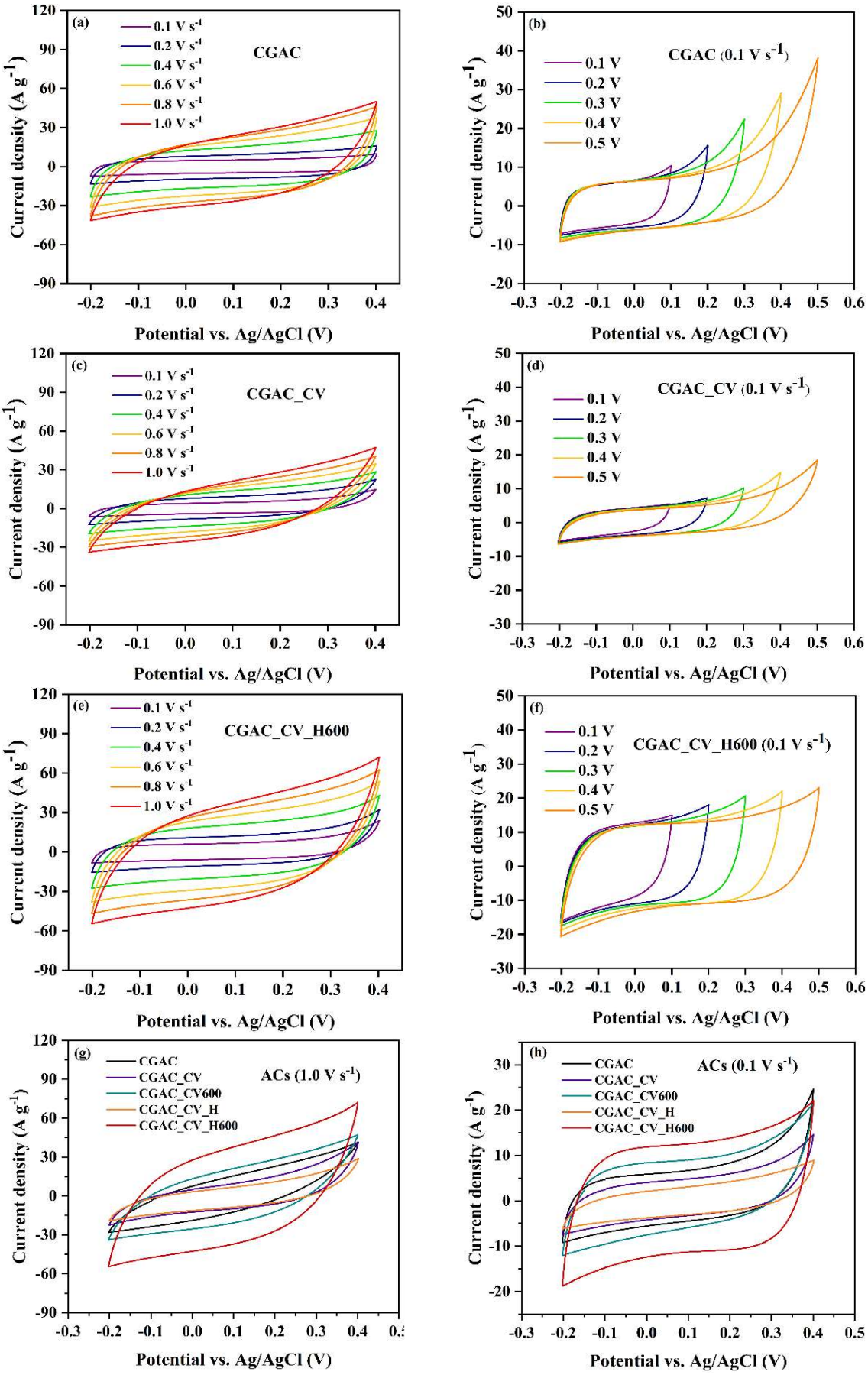

Figure 4. CV curves of CGAC, CGAC_CV, and CGAC_CV_H600: (a, c, e) at various scan rates (0.1 V·s^{-1} to 1.0 V·s^{-1}), (b, d, f) at 0.1 V·s^{-1} under different potential windows, and (g, h) comparison of CV responses at 1.0 V·s^{-1} and 0.1 V·s^{-1}.

3.7 Adsorption isotherms

The adsorption behavior of crystal violet dye on CGAC was evaluated using four isotherm models of Langmuir, Freundlich, Temkin, and Dubinin-Radushkevich (D-R), as illustrated in Figure 3 (c-f) and summarized in Table 2. Among these, the Freundlich model provided the best fit to the experimental data with the highest correlation coefficient ($R^2 = 0.9712$), suggesting that the adsorption process occurs on a heterogeneous surface and involves multilayer adsorption [40]. The Freundlich constant ($K_F = 0.2560$ L·mg^{-1}) reflects moderate adsorption affinity, while the intensity parameter ($n = 1.9125$) being greater than 1 indicates a favorable adsorption process [40]

In contrast, the Langmuir model, which assumes monolayer adsorption on a homogeneous surface, yielded a slightly lower correlation ($R^2 = 0.8917$), with the calculated maximum adsorption capacity ($q_{max} = 151.52$ mg·g^{-1}). This relatively high q_{max} value supports the strong adsorption potential of CGAC, although the deviation from ideal monolayer behavior implies surface heterogeneity [41]. The Temkin model also showed a strong linear fit ($R^2 = 0.8984$), indicating the presence of adsorbate-adsorbent interactions, where the adsorption heat decreases linearly with surface coverage [42]. The Temkin constant $B_1 = 32.7584$ J·mol^{-1} further confirms the chemisorptive nature of the interaction.

The D-R isotherm, while less correlated ($R^2 = 0.7516$), provides insight into the adsorption mechanism. The mean free energy (E) calculated from the D-R model was 0.5690 kJ·mol^{-1}, which is much less than 8 kJ·mol^{-1}, suggesting that physisorption predominates [43]. Taken together, the superior fit of the Freundlich and Temkin models indicates that the adsorption of crystal violet onto CGAC is best described as a multilayer physical adsorption process on a heterogeneous surface, with moderate interaction energies.

3.8 Cyclic voltametric (CV) Analysis

The Cyclic Voltammetry (CV) graph illustrates the relationship between potential (vs. Ag/AgCl) and current density using activated carbon (AC) as the electrode. It compares different amounts of adsorbent used for the removal of Crystal Violet dye. Figure 4 presents the CV measurements conducted in a 6 M KOH solution within a potential window of 0.4 V at a scan rate of 1.0 V·s^{-1}. The comparison includes the electrochemical performance of ACs. Furthermore, the total area under the CV curve corresponds to the total charge associated with the electrochemical process. It can be used to quantify the capacitive performance of the electrode. The specific capacitance (C) is calculated from CV curves using Equation (14) [44].

$$C = \left(\frac{I}{m \times s}\right) \tag{14}$$

$$C = \left(\frac{I \times \Delta t}{m \times \Delta V}\right) \tag{15}$$

where C represents the specific capacitance (F·g^{-1}) of the electrode materials, I (A) is the discharge current, s is the scan rate (V·s^{-1}), Δt (s) is the discharge time, m (g) is the mass of the ACs on the electrode, and ΔV (V) represents the working voltage.

The electrochemical behavior of the prepared activated carbon samples was investigated using cyclic voltammetry (CV), and the results are summarized in Figure 4. The CV curves were recorded at various scan rates (0.1 V·s^{-1} to 1.0 V·s^{-1}) and potential windows in a three-electrode Figure 4(a,c,e) show the CV curves of CGAC, CGAC_CV, and CGAC_CV_H600, respectively, at different scan rates.

Figure 4(a,c,e) show the CV curves of CGAC, CGAC_CV, and CGAC_CV_H600, respectively, at different scan rates. All samples exhibited quasi-rectangular CV profiles, characteristic of electric double-layer capacitor (EDLC) behavior. Notably, CGAC_CV_H600 displayed the largest enclosed area under the CV curve at all scan rates, indicating the highest specific capacitance and improved charge storage capacity. The shape of the CV curves remained relatively stable even at high scan rates (up to 1.0 V·s^{-1}), suggesting excellent rate capability and fast ion transport in the porous structure, particularly for the CGAC_CV_H600 sample. Figure 4(b,d,f) present the CV curves at 0.1 V·s^{-1} with increasing potential windows. The CGAC_CV_H600 electrode (Figure 4(f)) maintained a nearly rectangular shape up to 0.5 V, signifying good electrochemical stability and capacitive reversibility within the extended voltage window. In contrast, the CGAC (Figure 4(b)) showed noticeable distortion at higher potentials, possibly due to limited structural robustness or faradaic contributions.

Comparative CV analyses at high (1.0 V·s^{-1}) and low (0.1 V·s^{-1}) scan rates for all samples are shown in Figures 4(g,h). These curves provide critical insights into the electrochemical behavior and capacitive characteristics of the synthesized carbon materials. Ideally, electric double-layer capacitors (EDLCs) exhibit a nearly rectangular CV shape, reflecting efficient charge propagation and rapid ion diffusion [45]. All samples demonstrated quasi-rectangular CV curves at both scan rates, confirming EDLC-type behavior, where charge storage occurs primarily through non-Faradaic ion adsorption/desorption at the electrode-electrolyte interface. However, slight distortions from the ideal rectangular shape particularly noticeable in CGAC_CV and CGAC_CV_H suggest the occurrence of Faradaic reactions. These can be attributed to the incorporation of oxygen- and nitrogen-containing functional groups introduced during Crystal Violet (CV) dye modification and hydrothermal treatment [46]. Such functionalities contribute additional pseudocapacitive effects, thereby enhancing the overall charge storage capacity. Significantly, CGAC_CV_H600 consistently exhibits the largest enclosed CV area at both scan rates, indicating superior specific capacitance. This electrochemical behavior is well supported by the textural characteristics summarized in Table 1. CGAC_CV_H600 possesses the highest BET surface area (471.32 m^2·g^{-1}) and the largest pore volume (0.24 cm^3·g^{-1}), which together offer an extensive electrochemically accessible surface and facilitate ion transport within the porous network. The average pore diameter (1.61 nm) also lies within the optimal mesoporous range for EDLC applications [47]. At the high scan rate of 1.0 V·s^{-1} (Figure 4(g)), CGAC_CV_H600 demonstrates the highest current response, signifying excellent rate capability and fast ion kinetics. In contrast, CGAC_CV and CGAC_CV_H, which exhibit relatively lower surface areas (296.58 m^2·g^{-1} and 248.70 m^2·g^{-1}, respectively) and smaller pore volumes, show diminished current responses, highlighting the critical role of textural optimization in enhancing electrochemical performance. Even at the slower scan rate of 0.1 V·s^{-1} (Figure 4(h)), where overall current densities decrease

due to lower ion mobility, CGAC_CV_H600 still maintains the largest CV loop area. This consistent behavior across scan rates confirms its improved capacitive performance, attributed to the synergistic effect of hydrothermal treatment and subsequent carbonization at 600°C. Thus, the findings confirm that tailoring the physicochemical structure of CGAC via CV dye adsorption, hydrothermal treatment, and thermal activation can significantly improve capacitive properties by balancing electric double-layer and pseudocapacitive contributions.

3.9 Galvanostatic charge/discharge (GCD)

The galvanostatic charge/discharge (GCD) is an important & commonly used technique. It is usually distinguishing the principal charge storage mechanism, whether adsorption/desorption or pseudo-capacitive supercapacitor. The GCD curves of symmetric capacitors consist of CGAC, CGAC_CV and CGAC_CV_H600 employing 6 M KOH electrolyte under different current densities at 0.25 $A \cdot g^{-1}$ are depicted in Figure 5(a-c). While the specific capacitance, energy density and power density values calculated from GCD curves of both electrode materials are depicted in Figure 5(d), respectively. The GCD curves of CGAC, CGAC_CV and CGAC_CV_H600 are not perfect triangle shape, indicating that the charge storage is contributed by both EDLC and pseudocapacitance mechanisms [48,49]. The specific capacitance (C, $F \cdot g^{-1}$) of CGAC, CGAC_CV and CGAC_CV_H600 can be calculated by using the following Equations (15).

GCD curves exhibit a nearly symmetric triangular shape, characteristic of ideal electric double-layer capacitive (EDLC) behavior, suggesting reversible charge-discharge processes [50]. Among the three samples, CGAC_CV_H600 (Figure 5(c)) demonstrates the longest discharge times at all current densities, indicating superior capacitive performance. This enhancement is attributed to the combined effects of nitrogen and oxygen doping introduced via dye adsorption and the subsequent thermal treatment at 600°C, which likely improves conductivity, introduces more active sites, and optimizes pore structure [51,52]. In contrast, the dye-adsorbed sample CGAC_CV (Figure 5(b)) exhibits the shortest discharge duration and a more compressed GCD profile across all current densities, suggesting the lowest charge storage capability among the three materials. This decline in performance may be due to partial pore blockage by the adsorbed dye molecules and the absence of a post-treatment process to improve conductivity and restore porosity [53]. On the other hand, the unmodified CGAC (Figure 5(a)) shows intermediate behavior, indicating that although it lacks surface hetero-atoms, its porous network remains relatively accessible for ion transport. This allows for better charge retention compared to CGAC_CV, yet still falls short of the thermally treated CGAC_CV_H600, which demonstrates the highest capacitive performance due to enhanced conductivity and optimized surface chemistry.

As shown in Figure 5(d), the specific capacitance (C_{sp}) of CGAC_CV_ H600 reaches a maximum value of 326.42 $F \cdot g^{-1}$ at 0.25 $A \cdot g^{-1}$, decreasing to 178.33 $F \cdot g^{-1}$ at 1.00 $A \cdot g^{-1}$. This trend is consistent with the typical behavior of porous carbon electrodes, where lower current densities allow for more complete electrolyte ion diffusion into the porous network [54]. The CGAC and CGAC_CV samples exhibit lower C_{sp} values across all current densities, with CGAC showing a maximum of 201.5 $F \cdot g^{-1}$ and CGAC_CV only 95.72 $F \cdot g^{-1}$ at 0.25 $A \cdot g^{-1}$. These observations further support that the hydrothermal treatment facilitates structural and compositional enhancements necessary for high-performance supercapacitor electrod.

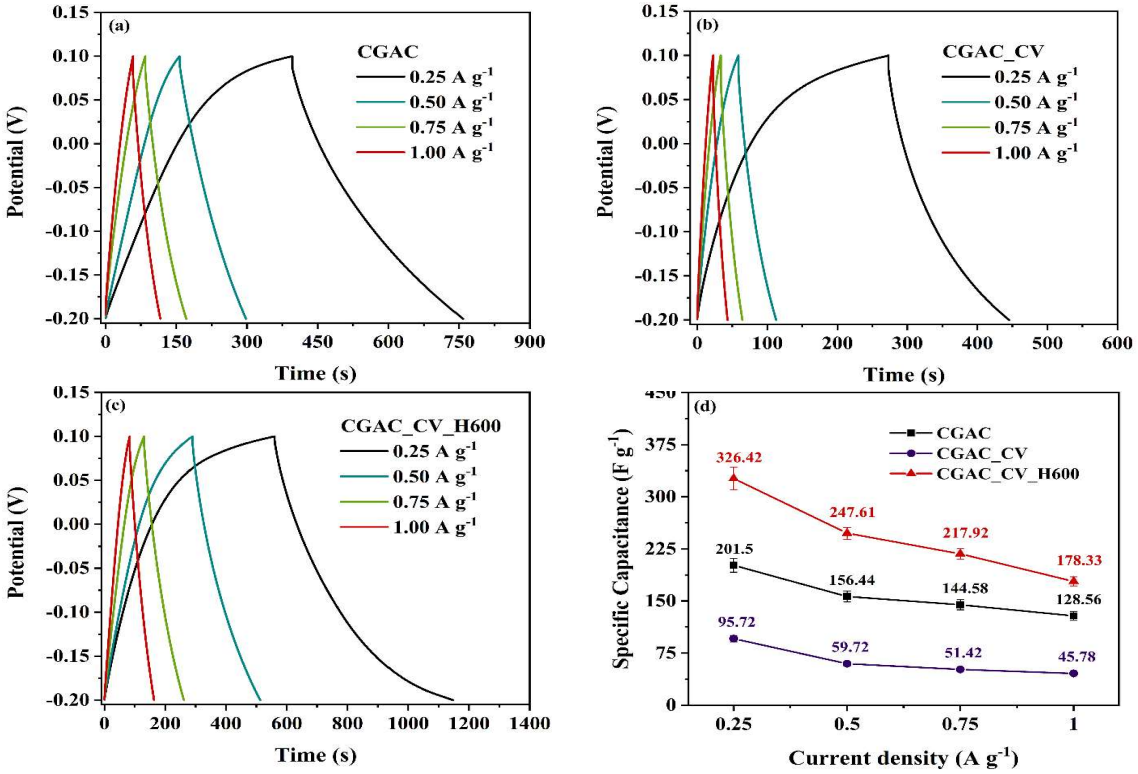

Figure 5. GCD curves of (a) CGAC, (b) CGAC_CV, and (c) CGAC_CV_H600 at 0.25-1.00 $A \cdot g^{-1}$; (d) specific capacitance versus current density for all samples.

Table 3. Comparative analysis of electrochemical performance parameters for biomass-derived carbon materials, the activating agents, incorporated dyes, heteroatoms, testing conditions, and specific capacitance values (C, $F \cdot g^{-1}$).

Biomass derived carbon	Activating agent	Dye	Heteroatoms	Electrolyte	Test condition [$A \cdot g^{-1}$]	C [$F \cdot g^{-1}$]	Ref.
Bamboo	KOH	MB	N, S	6 M KOH	0.5	491.2	[53]
Rice husk	KOH	MB	N, S	3 M H_2SO_4	0.5	127.9	[60]
Wheat straw	KOH	AZ	N, C, and O	1 M H_2SO_4	1	355.8	[61]
Anthracite coal	KOH	MB	N	6 M KOH	1	431.8	[55]
Ginkgo leaves	KOH	CR	N	1 M H_2SO_4	1	393	[56]
Ridge gourd	KOH	IND	N	1 M H_2SO_4	2	280	[62]
Coffee grounds	KOH	CV	N, O	6 M KOH	0.25	326.4	This study

To evaluate the electrochemical competitiveness of the CGAC_CV_H600 electrode, its performance was compared with previously reported biomass-derived carbon materials, as shown in Table 3. The table presents a side-by-side comparison based on precursor type, activating agent, incorporated dye, heteroatom doping, electrolyte, testing conditions, and the resulting specific capacitance values. Among the reported systems, bamboo-derived carbon activated with KOH and doped with nitrogen and sulfur, using methylene blue (MB) as the dye, exhibited the highest capacitance of 491.2 $F \cdot g^{-1}$ at 0.5 $A \cdot g^{-1}$ in 6 M KOH electrolyte [52]. Other materials, such as anthracite coal (431.8 $F \cdot g^{-1}$) [55] and ginkgo leaves (393 $F \cdot g^{-1}$) [56], also showed high specific capacitance, primarily due to the synergy of hierarchical porosity, high conductivity, and effective heteroatom doping.

In this study, coffee ground-derived activated carbon (CGAC_CV_H600) modified with crystal violet (CV) and carbonized at 600°C in KOH electrolyte exhibited a specific capacitance of 326.4 $F \cdot g^{-1}$ at 0.25 $A \cdot g^{-1}$, which is highly competitive with other biomass-based carbon materials. The relatively high performance can be attributed to the dual role of the dye: (1) as a nitrogen- and oxygen-containing source for heteroatom doping, and (2) as a structural modifier to create accessible porosity upon thermal decomposition. While the absolute capacitance values of CGAC_CV_H600 are lower than some of the highest-reported systems, the simplicity of the preparation, availability of raw material (spent coffee grounds), and the use of an environmentally benign activation process offer clear advantages in terms of sustainability and scalability. Moreover, the performance under mild electrolyte conditions (6 M KOH) and low current density reveals its strong potential for practical energy storage devices.

Crystal violet (CV) is a cationic triphenylmethane dye with a conjugated aromatic structure and multiple amine functional groups. During the adsorption process, the π-conjugated system of CV allows strong π–π interactions with the graphitic domains of activated carbon, while the presence of tertiary amines facilitates electrostatic and hydrogen bonding with oxygen-containing surface functionalities (e.g., –COOH, –OH) on CGAC [57]. These interactions not only immobilize the dye on the carbon surface but also introduce nitrogen heteroatoms into the matrix. Upon subsequent thermal or hydrothermal treatment, partial decomposition and rearrangement of the CV molecules result in the formation of N- and O-doped carbonaceous domains. The incorporated nitrogen atoms, particularly pyrrolic-N and graphitic-N types (as often reported in similar systems), can contribute additional redox-active sites [58]. These sites participate in faradaic reactions during the charge-discharge process, thereby introducing a pseudo-capacitive component in addition to the electric double-layer capacitance (EDLC) mechanism [59]. Moreover, the aromatic backbone of CV may facilitate electron delocalization and improve charge transport across the carbon surface [60]. This effect is particularly evident in the CGAC_CV_H600 sample, where the combination of heteroatom doping and optimized porosity leads to an increase in specific capacitance. The contribution of pseudocapacitance is supported by the slight deviation from ideal rectangular CV curves and the presence of redox-like features in GCD profiles. Thus, CV serves not only as an adsorbate but also as a chemical modifier that enriches the carbon matrix with electrochemically active functionalities, promoting a synergistic enhancement in overall charge storage through dual EDLC-pseudocapacitive mechanisms.

These findings confirm that waste-derived carbon from spent coffee grounds, when engineered through dye modification and thermal activation, can rival or exceed the performance of more complex biomass precursors and synthetic composites, highlighting its promise as a cost-effective and eco-friendly electrode material for supercapacitor applications.

4. Conclusion

This study establishes a sustainable pathway for transforming spent coffee grounds into multifunctional carbon materials applicable to both dye removal and energy storage. Under optimal operating conditions (0.5 g dosage, 300 $mg \cdot L^{-1}$ CV, 30°C, 120 min), the prepared activated carbon (CGAC) achieved a removal efficiency of 91.41%, with adsorption behavior consistent with pseudo-second-order kinetics and the Freundlich isotherm, confirming a spontaneous and endothermic nature. The reusability assessment further revealed that CGAC retained more than 88% of its initial performance after seven cycles, reflecting its durability and promise for practical wastewater treatment. Furthermore, the dye-loaded carbon was successfully repurposed into electrode materials through various post-treatment routes; unmodified CGAC, dye-loaded CGAC (CGAC_CV), hydrothermally treated (CGAC_CV_H), thermally treated (CGAC_CV_600), and combined hydrothermal-thermal treated (CGAC_CV_H600). Among these, the hydrothermal–thermal treated sample demonstrated the highest electro-chemical performance, reaching a specific capacitance of 326.4 $F \cdot g^{-1}$ at 0.25 $A \cdot g^{-1}$, owing to its optimized porosity and heteroatom doping. Overall, the findings highlight a circular approach that integrates wastewater remediation with the production of high-value energy storage materials, offering an effective solution to both environmental and energy-related challenges.

Acknowledgements

This work was supported by National Higher Education, Science, Research and Innovation Policy Council, Thaksin University (Fundamental Research Fund; TSU-68A105000078) Fiscal Year 2025. The authors would like to thank the Department of Chemistry, Faculty of Science and Digital Innovation, Thaksin University, for providing research facilities.

References

[1] J. Meena, S. shankari Sivasubramaniam, E. David, and S. K, "Green supercapacitors: review and perspectives on sustainable template-free synthesis of metal and metal oxide nanoparticles," *RSC Sustainability*, vol. 2, no. 5, pp. 1224-1245, 2024.

[2] C. Karaman, O. Karaman, N. Atar, and M. L. Yola, "Sustainable electrode material for high-energy supercapacitor: biomass-derived graphene-like porous carbon with three-dimensional hierarchically ordered ion highways," *Physical Chemistry Chemical Physics*, vol. 23, no. 22, pp. 12807-12821, 2021.

[3] D. V. Chernysheva, N. V. Smirnova, and V. P. Ananikov, "Recent trends in supercapacitor research: Sustainability in energy and materials," *ChemSusChem*, vol. 17, no. 5, p. e202301367, 2024.

[4] G. Hristea, M. Iordoc, E.-M. Lungulescu, I. Bejenari, and I. Volf, "A sustainable bio-based char as emerging electrode material for energy storage applications," *Scientific Reports*, vol. 14, no. 1, p. 1095, 2024.

[5] T. Temesgen, E.T. Bekele, B. A. Gonfa, L. T. Tufa, F. K. Sabir, S. Tadesse, and Y.Dessie, "Advancements in biomass derived porous carbon materials and their surface influence effect on electrode electrochemical performance for sustainable super-capacitors: A review," *Journal of Energy Storage*, vol. 73, p. 109293, 2023.

[6] S. Wang, Z. Ren, J. Li, Y. Ren, L. Zhao, and J. Yu, "Cotton-based hollow carbon fibers with high specific surface area prepared by ammonia etching for supercapacitor application," *RSC Advances*, vol. 4, no. 59, pp. 31300-31307, 2014.

[7] N. Kumar, S.-B. Kim, S.-Y. Lee, and S.-J. Park, "Recent advanced supercapacitor: A review of storage mechanisms, electrode materials, modification, and perspectives," *Nanomaterials (Basel)*, vol. 12, no. 20, p. 3708, 2022.

[8] H. Ji, X. Zhao, Z. Qiao, J. Jung, Y. Zhu, Y. Lu, L. L. Zhang, A. H. MacDonald, and R. S. Ruoff, "Capacitance of carbon-based electrical double-layer capacitors," *Nature Communications*, vol. 5, no. 1, p. 3317, 2014.

[9] R. Li, Y. Zhou, W. Li, J. Zhu, and W. Huang, "Structure engineering in biomass-derived carbon materials for electro-chemical energy storage," *Research (Wash D C)*, vol. 2020, p. 8685436, 2020.

[10] E. Huarote-Garcia, A. A. C. Riojas, I. E. Monje, E. O. López, O. M. A. Pinedo, G. A. Planes, and A. M. Baena-Moncada, "Activated carbon electrodes for supercapacitors from purple corncob (Zea maysL.)," *ACS Environmental Au*, vol. 4, no. 2, pp. 80-88, 2024.

[11] Z. Liu, S. Zhang, L. Wang, T. Wei, Z. Qiu, and Z. Fan, "High-efficiency utilization of carbon materials for supercapacitors," *Nano Select*, vol. 1, no. 2, pp. 244-262, 2020.

[12] M. Pathak, D. Bhatt, R. C. Bhatt, B. S. Bohra, G. Tatrari, S. Rana, M. C. Arya, and N. G. Sahoo, "High energy density supercapacitors: An overview of efficient electrode materials, electrolytes, design, and fabrication," *The Chemical Record*, vol. 24, no. 1, p. e202300236, 2023.

[13] A. A. Ahmad, M. A. Gondal, M. Hassan, R. Iqbal, S. Ullah, S. Alzahrani, W. A. Memon, F. Mabood, and S. Melhi, "Preparation and characterization of physically activated carbon and its energetic application for all-solid-state supercapacitors: A case study," *ACS Omega*, vol. 8, no. 24, pp. 21653-21663, 2023.

[14] S. M. Omokafe, A. A. Adeniyi, E. O. Igbafen, S. R. Oke, and P. A. Olubambi, "Fabrication of activated carbon from coconut shells and its electrochemical properties for supercapacitors," *International Journal of Electrochemical Science*, vol. 15, no. 11, pp. 10854-10865, 2020.

[15] Q. Xu, P. Cai, X. Ni, Y. Zhao, D. Li, Y. Chen, and H. Yuan, "Pyrolysis of loofah sponge into N/O self-doped three-dimensional porous carbon for supercapacitor," *Journal of Energy Storage*, vol. 109, p. 115180, 2025.

[16] K. Li, J. Luo, M. Wei, X. Yao, Q. Feng, X. Ma, and Z, Liu, "Functional porous carbon derived from waste eucalyptus bark for toluene adsorption and aqueous symmetric supercapacitors," *Diamond and Related Materials*, vol. 127, p. 109196, 2022.

[17] K. Kanjana, P. Harding, T. Kwamman, W. Kingkam, and T. Chutimasakul, "Biomass-derived activated carbons with extremely narrow pore size distribution via eco-friendly synthesis for supercapacitor application," *Biomass and Bioenergy*, vol. 153, p. 106206, 2021.

[18] S. R. Manippady, M. Michalska, M. Krajewski, K. Bochenek, M. Basista, A. Zaszczynska, T. Czeppe, L. Rogal, and A. Jain, "One-step synthesis of a sustainable carbon material for high performance supercapacitor and dye adsorption applications," *Materials Science and Engineering: B*, vol. 297, p. 116766, 2023.

[19] E. Taer, A. Apriwandi, and R. Taslim, "Heteroatom-doped biomass-derived porous carbon for supercapacitor applications: A review," *Trends in Sciences*, vol. 22, no. 8, Art. no. 8, 2025.

[20] S. Ghosh, S. Barg, S. M. Jeong, and K. (Ken) Ostrikov, "Heteroatom-doped and oxygen-functionalized nanocarbons for high-performance supercapacitors," *Advanced Energy Materials*, vol. 10, no. 32, p. 2001239, 2020.

[21] J. Wang, T. Huo, Y. Zhao, R. Lu, and X. Wu, "Recent advances in heteroatoms-doped porous carbon electrode materials for supercapacitors: A review," *Journal of Energy Storage*, vol. 110, p. 115216, 2025.

[22] M. Jalalah, H. Han, A. K. Nayak, and F. A. Harraz, "High-performance supercapacitor based on self-heteroatom-doped porous carbon electrodes fabricated from Mikania micrantha," *Advanced Composites and Hybrid Materials*, vol. 7, no. 1, p. 20, 2024.

[23] D. Mohan, A. Sarswat, Y. S. Ok, and C. U. Pittman, "Organic and inorganic contaminants removal from water with biochar,

a renewable, low cost and sustainable adsorbent – A critical review," *Bioresource Technology*, vol. 160, pp. 191-202, 2014.

[24] A. Ahmadpour, and D. D. Do, "The preparation of activated carbon from macadamia nutshell by chemical activation," *Carbon*, vol. 35, no. 12, pp. 1723-1732, 1997.

[25] J. Guo, and A. C. Lua, "Textural and chemical characterisations of activated carbon prepared from oil-palm stone with H_2SO_4 and KOH impregnation," *Microporous and Mesoporous Materials*, vol. 32, no. 1, pp. 111-117, 1999.

[26] B. M. Thamer, F. A. Al-aizari, and H. S. Abdo, "Enhanced adsorption of textile dyes by a novel sulfonated activated carbon derived from pomegranate peel waste: Isotherm, Kinetic and thermodynamic study," *Molecules*, vol. 28, no. 23, p. 7712, 2023.

[27] J. Saleem, Z. K. B. Moghal, S. Pradhan, and G. McKay, "High-performance activated carbon from coconut shells for dye removal: Study of isotherm and thermodynamics," *RSC Advances.*, vol. 14, no. 46, pp. 33797-33808, 2024.

[28] Y. Yao, H. Zuo, Y.Liu, S. Pang, L. Lan, F.Yao, Y. Wu, and Z. Liu, "Efficient dye adsorption of mesoporous activated carbon from bamboo parenchyma cells by phosphoric acid activation," *RSC Advances*, vol. 14, no. 18, pp. 12873-12882, 2024.

[29] A. Husain, K. Ansari, D. K. Mahajan, M. Kandasamy, M. N. M. Ansari, J. Giri, and H. A. Al-Lohedan, "Harnessing sustainable N-doped activated carbon from walnut shells for advanced all-solid-state supercapacitors and targeted Rhodamine B dye adsorption," *Journal of Science: Advanced Materials and Devices*, vol. 9, no. 2, p. 100699, 2024.

[30] J. Chupirom, S. Khaophong, N. Hemyakorn, S. Intachai, and P. Kongsune, "Arginine-modified surface coffee grounds activated carbon for Pb^{2+} adsorption: Kinetic, isotherm and thermodynamic studies," *Journal of Metals, Materials and Minerals*, vol. 35, no. 1, Art. no. 1, 2025.

[31] B. Weerasuk, T. Chutimasakul, N. Prigyai, and T. Sangtawesin, "Enhanced dye removal and supercapacitor performance of polyethyleneimine-impregnated activated carbon derived from local eucalyptus biochar," *RSC Sustainability*, vol. 3, no. 2, pp. 904-913, 2025.

[32] P. Treeweranuwat, P. Boonyoung, M. Chareonpanich, and K. Nueangnoraj, "Role of nitrogen on the porosity, surface, and electrochemical characteristics of activated carbon," *ACS Omega*, vol. 5, no. 4, pp. 1911-1918, 2020.

[33] T. Kangkamano, P. Kongsune, K. Suwanraksa, T. Charoenlap, S. Khaophong, and S. Intachai, "Effect of temperature of boric acid-doped porous activated carbon preparation on the electrochemical capacitor performance," *ScienceAsia*, vol. 51, no. 2, p. 1, 2025.

[34] M. J. Mostazo-López, J. Krummacher, A. Balducci, E. Morallón, and D. Cazorla-Amorós, "Electrochemical performance of N-doped superporous activated carbons in ionic liquid-based electrolytes," *Electrochimica Acta*, vol. 368, p. 137590, 2021.

[35] U. Baig, M. K. Uddin, and M. A. Gondal, "Removal of hazardous azo dye from water using synthetic nano adsorbent: Facile synthesis, characterization, adsorption, regeneration and design of experiments," *Colloids and Surfaces A: Physicochemical and Engineering Aspects*, vol. 584, p. 124031, 2020.

[36] S. Bentahar, A. Dbik, M. E. Khomri, N. E. Messaoudi, and A. Lacherai, "Adsorption of methylene blue, crystal violet and congo red from binary and ternary systems with natural clay: Kinetic, isotherm, and thermodynamic," *Journal of Environmental Chemical Engineering*, vol. 5, no. 6, pp. 5921-5932, 2017.

[37] A. H. Jawad, A. S. Abdulhameed, M. A. K. M. Hanafiah, Z. A. ALOthman, M. R. Khan, and S. N. Surip, "Numerical desirability function for adsorption of methylene blue dye by sulfonated pomegranate peel biochar: Modeling, kinetic, isotherm, thermodynamic, and mechanism study," *Korean Journal of Chemical Engineering*, vol. 38, no. 7, pp. 1499-1509, 2021.

[38] A. H. Jawad, A. S. Abdulhameed, N. N. Bahrudin, N. N. M. F. Hum, S. N. Surip, S. S. A. Syed-Hassan, E. Yousif, and S. Sabar, "Microporous activated carbon developed from KOH activated biomass waste: Surface mechanistic study of methylene blue dye adsorption," *Water Science and Technology*, vol. 84, no. 8, pp. 1858-1872, 2021.

[39] L. P. Lingamdinne, S. K. Godlaveeti, G. K. R. Angaru, Y.-Y. Chang, R. R. Nagireddy, A. R. Somala, and J. R. Koduru, "Highly efficient surface sequestration of Pb^{2+} and Cr^{3+} from water using a Mn_3O_4 anchored reduced graphene oxide: Selective removal of Pb^{2+} from real water," *Chemosphere*, vol. 299, p. 134457, 2022.

[40] H. Freundlich, "Über die adsorption in Lösungen," *Zeitschrift für Physikalische Chemie*, vol. 57U, no. 1, pp. 385-470, 1907.

[41] I. Langmuir, "The adsorption of gases on plane surfaces of glass, mica and platinum," *Journal of the American Chemical Society*, vol. 40, no. 9, pp. 1361-1403, 1918.

[42] K. H. Chu, "Revisiting the temkin isotherm: Dimensional inconsistency and approximate forms," *Industrial & Engineering Chemistry Research*, vol. 60, no. 35, pp. 13140-13147, 2021.

[43] M. M. Dubinin, "The potential theory of adsorption of gases and vapors for adsorbents with energetically nonuniform surfaces.," *Chemical Reviews*, vol. 60, no. 2, pp. 235-241, 1960.

[44] K. Surya, and M. S. Michael, "Hierarchical porous activated carbon prepared from biowaste of lemon peel for electrochemical double layer capacitors," *Biomass and Bioenergy*, vol. 152, p. 106175, 2021.

[45] P. Simon, and Y. Gogotsi, "Materials for electrochemical capacitors," *Nature Materials*, vol. 7, no. 11, pp. 845-854, 2008.

[46] J. Chmiola, G. Yushin, Y. Gogotsi, C. Portet, P. Simon, and P. L. Taberna, "Anomalous increase in carbon capacitance at pore sizes less than 1 nanometer," *Science*, vol. 313, no. 5794, pp. 1760-1763, 2006.

[47] Y. Zhai, Y. Dou, D. Zhao, P. F. Fulvio, R. T. Mayes, and S. Dai, "Carbon materials for chemical capacitive energy storage," *Advanced Materials*, vol. 23, no. 42, pp. 4828-4850, 2011.

[48] J. Li, Y. Sun, X. Jia, Y. Chen, Y. Tang, P. Wan, and J. Pan, "Boron, oxygen co-doped porous carbon derived from waste tires with enhanced hydrophilic interface as sustainably high-performance material for supercapacitors," *Journal of Energy Storage*, vol. 80, p. 110320, 2024.

[49] K. Thongkam, N. Chaiyut, M. Panapoy, and B. Ksapabutr, "Biomass-based nitrogen-doped carbon/polyaniline composite as electrode material for supercapacitor devices," *Journal of Metals, Materials and Minerals*, vol. 33, no. 3, pp. 1675-1675, 2023.

[50] K. C. S. Lakshmi, and B. Vedhanarayanan, "High-performance supercapacitors: A comprehensive review on paradigm shift of conventional energy storage devices," *Batteries*, vol. 9, no. 4, p. 202, 2023.

[51] M. Sevilla, and A. B. Fuertes, "The production of carbon materials by hydrothermal carbonization of cellulose," *Carbon*, vol. 47, no. 9, pp. 2281-2289, 2009.

[52] L. L. Zhang, and X. S. Zhao, "Carbon-based materials as supercapacitor electrodes," *Chemical Society Reviews*, vol. 38, no. 9, pp. 2520-2531, 2009.

[53] W. Tong, F. Huang, L. Chen, H. Wu, and X. Zhou, "Methylene blue enhanced bamboo activated carbon as high performance supercapacitor electrode materials," *Industrial Crops and Products*, vol. 180, p. 114786, 2022.

[54] D.-W. Wang, F. Li, M. Liu, G. Q. Lu, and H.-M. Cheng, "3D aperiodic hierarchical porous graphitic carbon material for high-rate electrochemical capacitive energy storage," *Angewandte Chemie International Edition*, vol. 47, no. 2, pp. 373-376, 2008.

[55] G. Lv, X. Dai, Y. Qiao, Q. Tan, Y. Liu, and Y. Chen, "Functional combination of methylene blue and porous carbon mutually promotes to deliver ultrahigh rate capacitive and energy storage performance," *Chemical Engineering Journal*, vol. 448, p. 137660, 2022.

[56] H. Xu, Y. Bao, S. Zuo, P. Chen, Y. Zhu, X. Kong, and Y, Chen, "Enhanced electrochemical performance of biomass porous carbon adsorption congo red," *Journal of The Electrochemical Society*, vol. 169, no. 1, p. 010514, 2022.

[57] I. Loulidi, F. Boukhlifi, M. Ouchabi, A. Amar, M. Jabri, A. Kali, S. Chraibi, C. Hadey, and F. Aziz, "Adsorption of crystal violet onto an agricultural waste residue: kinetics, isotherm, thermodynamics, and mechanism of adsorption," *ScientificWorldJournal*, vol. 2020, p. 5873521, 2020.

[58] A. Aldalbahi, B. M. Thamer, M. Rahaman, and M. H. El-Newehy, "Self-nitrogen-doped nanoporous carbons derived from poly(1,5-diaminonaphthalene) for the removal of toxic dye pollutants from wastewater: Non-linear isotherm and kinetic analysis," *Polymers (Basel)*, vol. 12, no. 11, p. 2563, 2020.

[59] L. Zhong, L. Zhang, and H. Shi, "Adsorption of crystal violet onto nitrogen-doped mesoporous carbon," *Progress in Reaction Kinetics and Mechanism*, vol. 42, no. 3, pp. 269-281, 2017.

[60] T. Anusonthiwong, N. Suwatanapongched, J. Surawattanawiset, N. Chittreisin, S. Ittisanronnachai, T. Sangtawesin, and S. Anantachaisilp, "Activated carbon derived from rice husks enhanced by methylene blue and gamma irradiation for supercapacitor applications," *RSC Sustainability*, vol. 3, no. 3, pp. 1507-1515, 2025.

[61] Y. Bao, J. Ma, H. Xu, Z. Yang, M. Liu, and Y. Chen, "Polymerization of redox-active alizarin in biomass porous carbon with enhanced cycling stability for supercapacitor," *Journal of Energy Storage*, vol. 102, p. 114172, 2024.

[62] S. Brahma, and K. Ramanujam, "Combination of redox-active natural indigo dye and bio-derived carbon from ridge gourd fruit for high-performance asymmetric supercapacitors," *Ionics*, vol. 28, no. 3, pp. 1427-1440, 2022.